Hindawi
Mathematical Problems in Engineering
Volume 2019, Article ID 8982028, 14 pages
https://doi.org/10.1155/2019/8982028

Research Article

Dynamical Analysis and Stabilization of Wind Turbine Drivetrain via Adaptive Fixed-Time Terminal Sliding Mode Controller

Jianxiang Yang,[1,2] Anle Mu ,[1] and Nailu Li [3]

[1]*School of Mechanical and Precision Instrument Engineering, Xi'an University of Technology, Xi'an 710048, China*
[2]*School of Mechanical and Electrical Engineering, Hezhou University, Hezhou 542899, China*
[3]*School of Hydraulic, Energy and Power Engineering, Yangzhou University, Yangzhou, Jiangsu, 225127, China*

Correspondence should be addressed to Anle Mu; muanle@xaut.edu.cn

Received 7 April 2019; Revised 10 June 2019; Accepted 23 June 2019; Published 22 July 2019

Academic Editor: Leonardo Acho

In order to study the stability of the wind turbine drivetrain in further depth, we present a nonlinear relative rotation mathematical model considering the nonlinear time-varying stiffness and the nonlinear damping force. Meanwhile, the nonlinear dynamics of the model under combined harmonic excitation are studied in detail. And some interesting dynamic phenomena are observed visually. Furthermore, to suppress chaotic oscillation within bounded time independent of initial conditions, a novel adaptive fixed-time terminal sliding mode controller is proposed. The stability of the final closed loop system is guaranteed according to Lyapunov stability theory. Rigorous mathematical analyses are used to prove the validity of the presented approach. Finally, compared with the existing finite-time stability method, simulation results are given to highlight the effectiveness and superiority of the proposed method and verify the theoretical analyses.

1. Introduction

Two basic goals for wind energy conversion system (WECS) can be summarized as increasing its annual energy yield and extending its service life. Generally, in order to achieve the more annual energy production in a wide range of wind speeds, most of the research works regarding maximum power point tracking (MPPT) algorithms have been devoted to the main control strategies [1–3]. Boukhezzar et al. [4] used a two-mass wind turbine model to deal with the wind power capture optimization problem while restricting transient loads on the drivetrain components. However, from the operational lifetime of a wind turbine point of view, failure of the drivetrain components is currently listed among the most problematic failures. Hence, the stability and operational characteristics of wind turbine drivetrain have significant impact on the dynamics of the whole WECS, especially as it bears the amount of dynamic loads [5]. To prevent excessive drivetrain load and avoid the resonance, it is mentioned in [6] that a power-electronics-based controller was used to temporarily shift the closed loop eigenfrequency of the drivetrain through the addition of virtual inertia. Some effort has been dedicated to the small signal stability of wind turbine drivetrain with the two-mass model. Geng et al. [7] presented a torque compensation strategy and an active-damping strategy to improve the system stability in wind turbine drivetrain based on small-signal analysis. Chen et al. [8] proposed a power control strategy with damping injection for the suppression of natural resonant mode and the aerodynamic load, which is proportional to the small-signal value of the generator speed. Rahimi [9] analyzed small signal stability of the full WECS, designed corresponding controller elaborately, and theoretically examined impact of speed controller on the stability of the system connected to the power grid. Xie et al. [10] developed unified small-signal models to find out all types of oscillation modes and analyze the dynamic and steady-state behaviors in a two-mass shaft model for the mechanical system. Regarding torsional electromechanical oscillations, a wind turbine stabilizer (WTS) adding positive damping to suppress torsional vibrations in

the drivetrain system was implemented in [11]. Even though the dynamic behaviors of drivetrain system were described in the mentioned publications [12–14], due to highly fluctuating wind power generation, unpredictable demand, nonlinear power characteristics, etc., a fixed value of inertia gain may not contribute a satisfactory inertial response during each system event [15]. In addition, the existent contributions were basically modeled by linearized average dynamics. It should be noted that, with the help of nonlinear dynamics theory, Meng et al. [16] investigated bifurcation phenomenon of a kind of nonlinear-relative rotational system with combined harmonic excitation and did not offer a control approach to eliminate bifurcation features. Therefore, to our best knowledge, few works regarding the issue of the stability have been investigated in wind turbine drivetrain with combined harmonic excitation based on nonlinear dynamics theory. What is more is that it is of great significance to design an advanced control scheme with strong antidisturbance ability as well as being independent of the system's mathematical model.

The effective control of uncertain nonlinear dynamic systems has been a hot issue of academia. The various advanced control methods including feedback control [17], fuzzy control [18], adaptive control [19], and sliding mode control [20] have been studied to drive the dynamic system to the expected orbit or achieve these synchronization problems. Among these control strategies, the stability and secure operation of dynamic systems with uncertainties can all be guaranteed. In addition, all the previous methods cannot achieve system stability in finite time and only accomplish the asymptotic stability, which means that convergence time cannot be estimated in advance. Finite-time control [21] with better robustness, stronger anti-interface, and higher precision performance can ensure the system stability within bounded time. Sun et al. [22] applied the finite-time theory to deal with real combination synchronization problem between three complex-variable chaotic systems with unknown parameters. Yang et al. [23] studied the incorporation of periodically intermittent memory feedback control into finite-time stability theory to synchronize two chaotic systems with discrete and distributed delays.

However, an important limitation of finite-time control is that its stable time depends mainly on the initial condition of the system in the practical application. To compensate this drawback, Polyakov [24] pioneered the fixed-time stability method. In particular, Zuo further proposed the fixed-time stability theory in [25]. Compared with the finite-time stability, fixed-time stability possesses a faster convergence rate, higher precision estimation, and stronger disturbance rejection. The fixed-time stability of nonlinear systems with uncertain parameters, unmodeled dynamics, and unknown disturbances has been a well-established area [26–28]. Ma et al. [29] proposed an adaptive fixed-time fast terminal sliding mode control method for the second-order chaotic oscillation power system. In second-order uncertain dynamical system, Boukattay et al. [30] presented a robust and adaptive nonsingular fast terminal sliding mode (RANFTSM) control strategy for the tracking problem. At present, Hu et al. [31] investigated a new fixed-time stability theorem with high-precision estimation for dynamical systems. Therefore, motivated by the above analysis, we have proposed an adaptive fixed-time terminal sliding mode control method to handle the complex control problem in a better way. Furthermore, to the best of our knowledge, there is little literature on the control method of wind turbine drivetrain with combined harmonic excitation.

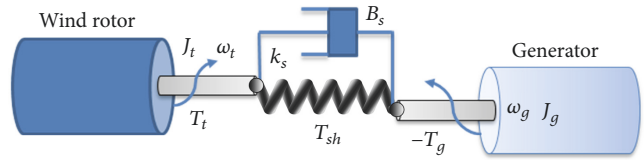

Figure 1: Two-mass drivetrain scheme.

The main innovations of this paper are summarized as follows. First, the wind turbine drivetrain model with the nonlinear time-varying stiffness and the nonlinear damping force is demonstrated in detail. Second, stability of wind turbine drivetrain is analyzed with and without considering external excitation according to Lyapunov stability theory. Dynamic characteristics of the system are depicted concretely by the aid of nonlinear dynamical theory. Third, an adaptive fixed-time terminal sliding mode controller is proposed for the suppression of chaotic oscillation in wind turbine drivetrain with combined harmonic excitation. The proposed control scheme can guarantee the system stabilization within fixed-time independent of initial value and have advantages in convergence rate and chattering problem. Finally, simulation results are given to demonstrate the effectiveness of the proposed approach.

The rest of this paper is organized as follows. In Section 2, we recall the two-mass model of wind turbine, and a new mathematical model of a typical wind energy drivetrain with nonlinear terms is presented. Stability of wind turbine drivetrain is comprehensively analyzed with and without considering external excitation in Section 3. The adaptive fixed-time terminal sliding mode controller is designed and the stability is analytically proved in Section 4. The numerical simulations are used to illustrate the validity of the obtained scheme in Section 5. The conclusions are given in Section 6.

2. Mathematical Model of Wind Turbine

The purpose of this section is to introduce the two-mass model based wind turbine drivetrain. Then, the wind turbine system including the blade, wind rotor, drivetrain, and generator is illustrated in Figure 1. The two-mass model can be commonly used in accommodating flexible modes that cannot be achieved by using the one-mass model in previous studies. In order to study the nonlinear characteristic of wind turbine on the grid, further modeling of wind turbine dynamics should receive great attention.

A typical configuration of variable-speed wind turbine drivetrain is illustrated in Figure 2. A two-mass model representation of the drivetrain is essential in order to correctly illustrate the dynamic impact of wind turbines on the grid [7]. In the two-mass model, the low speed mass of the turbine is

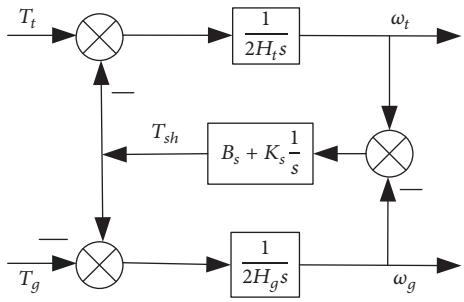

Figure 2: Two-mass model of drivetrain.

connected to the high speed mass of the generator through a flexible shaft modeled as a spring and damper [13]. In industrial practices, all values in the stated equations are converted to per unit system. The inertia moment of the rotor J can be represented by the per unit inertia constant H customarily in [15]:

$$2H = 2\frac{W_E}{S_m} = 2\frac{0.5J\omega_{s0}^2}{S_m} \approx J \tag{1}$$

where W_E, S_m, ω_{s0} denote the energy stored, the installed capacity, and the synchronous angular frequency in the per unit system, respectively.

Therefore, the inertia moment of turbine rotor J_t and generator rotor J_g can be, respectively, represented by the per unit inertia constants H_t, H_g. From Figure 2, the linearized mathematical expression of the two-mass drivetrain is described as follows:

$$\begin{aligned} 2H_t\dot{\omega}_t &= T_t - T_{sh} \\ 2H_g\dot{\omega}_g &= T_{sh} - T_g \\ T_{sh} &= k_s\varphi + B_s\left(\omega_t - \omega_g\right) \\ \dot{\varphi} &= \omega_b\left(\omega_t - \omega_g\right) \end{aligned} \tag{2}$$

where superscript _ denotes per unit (pu) value and H_g, H_t, ω_t, ω_g, T_g, T_t, T_{sh} denote the inertia constants of the generator and turbine (in sec), the turbine and generator speeds (in rad/sec), the generator electrical torque and the turbine mechanical torque (in pu), and the shaft torsional torque (in pu), respectively. And φ, k_s, B_s, ω_b denote the shaft twist angle (in rad), the shaft stiffness coefficient (in pu/elec. rad), the damping coefficient of the shaft (in pu), and the reference speed ($\omega_b = 314$ rad/sec), respectively.

From (2), the shaft twist angle can then be obtained:

$$\begin{aligned} &\ddot{\varphi} + B_s\left(\frac{1}{2H_t} + \frac{1}{2H_g}\right)\dot{\varphi} + \omega_b k_s\left(\frac{1}{2H_t} + \frac{1}{2H_g}\right)\varphi \\ &\quad = \omega_b\left(\frac{T_t}{2H_t} + \frac{T_g}{2H_g}\right) \end{aligned} \tag{3}$$

Considering (3) and according to the above explanations, the shaft natural oscillation frequency and damping ratio in the absence of external torque can be written as

$$\begin{aligned} \omega_n &= \sqrt{k_s\omega_b\left(\frac{1}{2H_t} + \frac{1}{2H_g}\right)}, \\ \varsigma &= \frac{B_s\left(1/2H_t + 1/2H_g\right)}{2\omega_n} \end{aligned} \tag{4}$$

The drivetrain of the 2 MW turbine generator has the following partial parameters [9]: $H_g = 0.6sec$, $H_t = 4sec$, $k_s = 0.6$pu/elec. rad, $B_s = 1$pu, $\omega_b = 314$ rad/sec; the natural oscillation frequency of the torsional modes is obtained equal to $\omega_n = 13.437$ rad/sec ($f_n = 2.139$Hz) with damping ratio of $\varsigma = 0.0357$. Since the damping ratio is far less than 1, the system is a typical underdamped system, and the torsional vibration of the shaft can be easily excited.

In the existing literatures [6, 8, 15, 32], there is a common approach to mitigate excessive drivetrain load through the addition of virtual inertia or damping ratio in the dynamic model. The dynamic of turbine speed is much slower and more difficult to control than that of the generator speed because of the huge turbine and generator inertias, and the main source of torsional vibration is electromagnetic torque. The transfer function from torsional angular velocity ($\dot{\varphi}$) to electromagnetic torque can be easily established in the small signal model of the drivetrain. And the neighborhood of the quasisteady operation point can be deduced ($\overline{\omega}_g = \overline{\omega}_t$) by the small signal model. However, different initial values of the small signal model can influence both frequency and damping ratio of the oscillation mode [10]. What is more is that, according to the above explanations, all dynamic behaviors are described under the linearized model.

In order to further study the dynamic characteristics, nonlinear time-varying stiffness and damping are used by equivalent principle in Figure 2, given by

$$T_{sh} = k\varphi + B_s\left(\omega_t - \omega_g\right) + B'_s\left(\omega_t - \omega_g\right)^3 \tag{5}$$

where $k = k_s(1 + k'\sin(\Omega t))$, B'_s is the nonlinear damping coefficient, Ω is the nonlinear stiffness excitation frequency, and k' is the nonlinear stiffness amplitude.

Combining (2) and (3), the Lagrangian dynamics equation after nonlinear terms injection can then be rewritten as

$$\ddot{\varphi} + \omega_n^2\varphi + k\varphi\cos(\Omega t) + a\dot{\varphi} + b\dot{\varphi}^3 = F(t) \tag{6}$$

where $a = B_s(1/2H_t + 1/2H_g)$, $b = (B'_S/\omega_b^2)(1/2H_t + 1/2H_g)$, $\omega_n = \sqrt{k_s\omega_b(1/2H_t + 1/2H_g)}$, $k = \omega_n^2 k'$, $\omega_b = 2\pi f = 2\pi \times 50$, $F(t) = (T_t/2H_t + T_g/2H_g)\omega_b$, and $F(t)$ is the lumped disturbance excitation.

From (6), this is a general equation of nonlinear dynamics and the basic principle of the two-mass relative rotation system in the wind turbine drivetrain. And it will be the basis for further study of the dynamic characteristics.

Table 1: The running state of system (11).

Number	Parameter	Eigenvalue	Root	Notes
1	$a < 0, a^2 - 4\omega_n^2 \geq 0$	$a \leq -2\omega_n$, $\mathrm{Re}\,\lambda > 0$	Two positive real roots	Instability
2	$a < 0, a^2 - 4\omega_n^2 < 0$	$-2\omega_n < a < 0$, $\mathrm{Re}\,\lambda > 0$	Two positive real roots	Instability
3	$a > 0, a^2 - 4\omega_n^2 \geq 0$	$a \geq 2\omega_n$, $\mathrm{Re}\,\lambda < 0$	Two negative real roots	Stability
4	$a > 0, a^2 - 4\omega_n^2 < 0$	$0 < a < 2\omega_n$, $\mathrm{Re}\,\lambda < 0$	Two negative real roots	Stability

3. Stability Analysis of Wind Turbine Drivetrain

When the wind turbine operates in rated conditions, an external disturbance excitation, such as the fluctuation of the random energy frequency or amplitude, will affect the stability of the system. Subsequently, the system will enter a new operating state. And there will be a complex transient process because of the nonlinearity of every part. The nonlinear dynamical behaviors along with the fluctuation of the amplitude of the shaft twist angle are particularly focused on.

3.1. Dynamic Characteristics of the Autonomous System. From (6), $x = \varphi$, the Euler equation of the natural oscillation (without external torque) can be listed:

$$\ddot{x} + a\dot{x} + b\dot{x}^3 + \omega_n^2 x + kx\cos(\Omega t) = 0 \tag{7}$$

According to the properties of the autonomous system [33], the system is an autonomous system without considering the time-varying stiffness of parameters. Then we have $\ddot{x} + a\dot{x} + b\dot{x}^3 + \omega_n^2 x = 0$, let $x = x_1$, $\dot{x} = x_2$. Equation (7) is rewritten as

$$\begin{aligned} \dot{x}_1 &= x_2 \\ \dot{x}_2 &= -ax_2 - bx_2^3 - \omega_n^2 x_1 \end{aligned} \tag{8}$$

Theorem 1. *For system (11), when $a < 0$, $b < 0$, it is unstable at the origin* O(0; 0)*; when $a > 0$, $b > 0$, it is asymptotically stable at the origin* O(0; 0).

Proof. According to system (11), the origin O (0; 0) is the only equilibrium point. Let $x_1 = p$, $x_2 = -\omega_n q$; one has

$$\begin{aligned} \dot{p} &= -\omega_n q \\ \dot{q} &= -aq - b\omega_n^2 q^3 + \omega_n p \end{aligned} \tag{9}$$

Consider the following Lyapunov positive definite function as $(p, q) = (1/2)(p^2 + q^2)$; the time derivative of $V(p, q)$ can be obtained as

$$\dot{V}(p,q) = \frac{\partial V}{\partial p}\dot{p} + \frac{\partial V}{\partial q}\dot{q} = -q^2\left(a + b\omega_n^2 q^2\right) \tag{10}$$

If $a < 0, b < 0, \dot{V}(p, q) > 0$, it is unstable at the origin O(0; 0); when a > 0, b $> 0, \dot{V}(p, q) < 0$, it is asymptotically stable at the origin O(0; 0). □

Theorem 2. *For system (11), when $b = 0$, $a < 0$, it is unstable at the origin* O(0; 0)*; when $b = 0$, $a > 0$, it is stable at the origin* O(0; 0)*; when $b = 0$, $a = 0$, closed trajectory bifurcation occurs at the origin* O(0; 0).

Proof. According to system (11), when $b = 0$, thus, it is rewritten as

$$\begin{aligned} \dot{x}_1 &= x_2 \\ \dot{x}_2 &= -ax_2 - \omega_n^2 x_1 \end{aligned} \tag{11}$$

The Jacobi matrix of system (14) can be further written as

$$J = \begin{bmatrix} 0 & 1 \\ -\omega_n^2 & -a \end{bmatrix} \tag{12}$$

The corresponding characteristic equation of Jacobi matrix J is $\lambda^2 + a\lambda + \omega_n^2 = 0$. It is clear that $\lambda_{1,2} = (-\mathrm{a} \pm \sqrt{\mathrm{a}^2 - 4\omega_\mathrm{n}^2})/2$ is the eigenvalue. Specific stability state is summarized in Table 1.

As shown in Figures 3 and 4, for system (11), when $b = 0$, $a < 0$, it is unstable at the origin O(0; 0); when $b = 0$, $a > 0$, it is stable at the origin O(0; 0); when $b = 0$, $a = 0$, closed trajectory bifurcation occurs at the origin O(0; 0). □

3.2. Dynamic Characteristics of the Nonautonomous System. Considering the combination harmonic excitation with unequal frequency, assume $(t) = f_1\cos(\nu_1 t) + f_2\cos(\nu_2 t)$; the differential equation of system (7) can be rewritten as

$$\begin{aligned} &\ddot{x} + a\dot{x} + b\dot{x}^3 + \omega_n^2 x + kx\cos(\Omega t) \\ &= f_1\cos(\nu_1 t) + f_2\cos(\nu_2 t) \end{aligned} \tag{13}$$

Adding a small parameter ζ to the nonlinear item, we get

$$\begin{aligned} &\ddot{x} + \zeta a\dot{x} + \zeta b\dot{x}^3 + \omega_n^2 x + \zeta kx\cos(\Omega t) \\ &= f_1\cos(\nu_1 t) + f_2\cos(\nu_2 t) \end{aligned} \tag{14}$$

The system (14) is analyzed using the multiscale method [34], and the solution of the system is assumed as

$$x(t,\zeta) = x_0(T_0, T_1) + \zeta x_1(T_0, T_1) \tag{15}$$

where $T_0 = t$, $T_1 = \zeta t$ denote the fast time-varying scale and the slow time-varying scale, respectively. Substituting (15) into (14), the coefficients of ζ^0, ζ^1 for the two sides of the equation can be recognized as equal. The perturbation equation can be obtained as

$$D_0^2 x_0 + \omega_n^2 x_0 = f_1\cos(\nu_1 T_0) + f_2\cos(\nu_2 T_0) \tag{16}$$

$$\begin{aligned} D_0^2 x_1 + \omega_n^2 x_1 = &-2D_0 D_1 x_0 - aD_0 x_0 - b(D_0 x_0)^3 \\ &- kx_0\cos(\Omega T_0) \end{aligned} \tag{17}$$

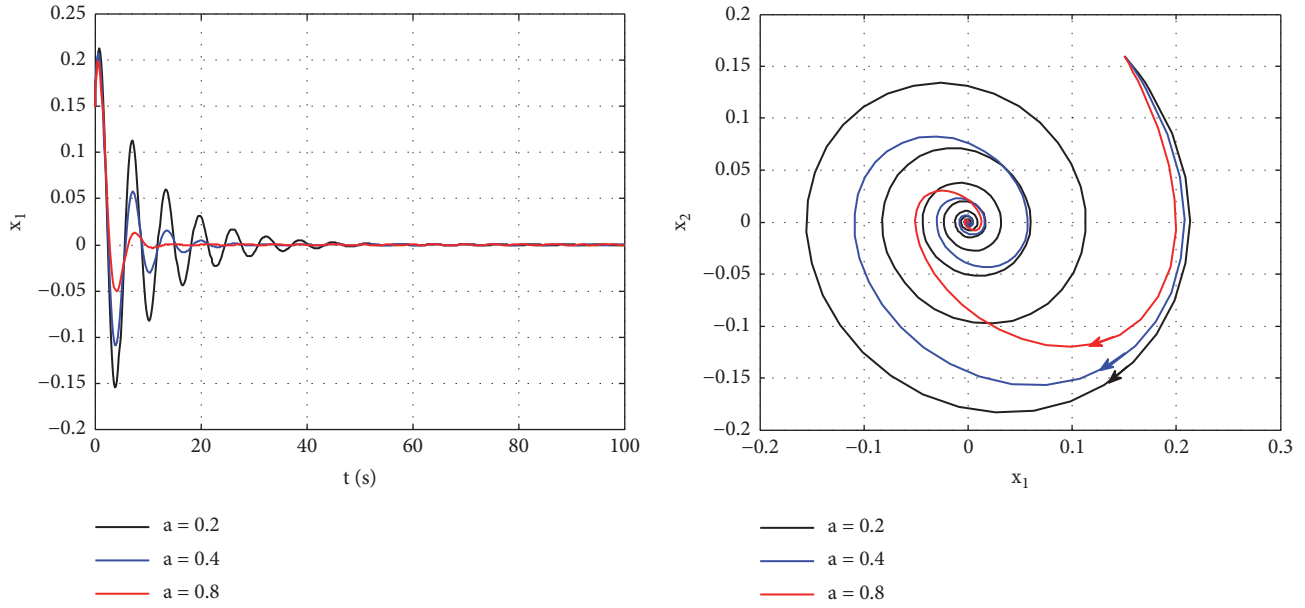

Figure 3: Time domain diagrams and phase portrait when $a > 0$.

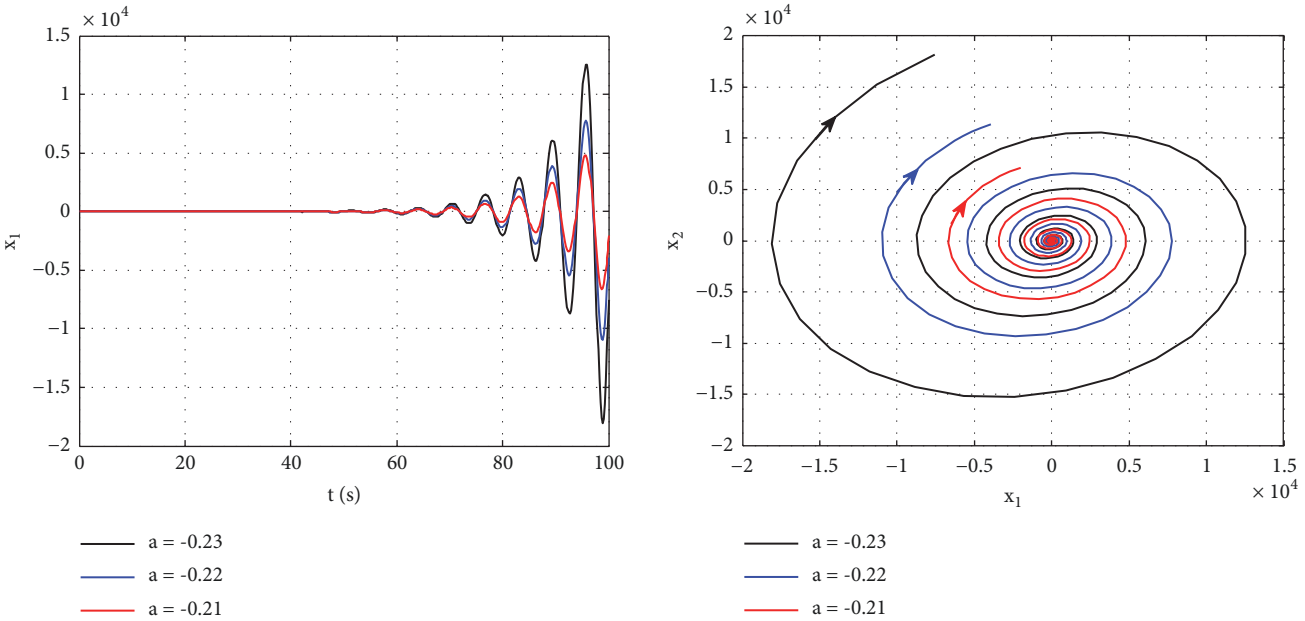

Figure 4: Time domain diagrams and phase portrait when $a < 0$.

where $D_i = \partial/\partial T_i (i = 0, 1)$ denotes the partial differential operator. General solution of (16) can be constructed:

$$x_0 = A(T_1) e^{i\omega_n T_0} + \Lambda_1 e^{i\nu_1 T_0} + \Lambda_2 e^{i\nu_2 T_0} + c.c.. \quad (18)$$

where $A, c.c.$ denote the pending complex function and conjugate items, respectively. $\Lambda_i = f_i/2(\omega_n^2 - \nu_i^2)$ $(i = 1, 2)$.

In order to simplify the calculation process without loss of generality, substituting (18) into (17), let $\Omega = \omega_n$, we found that there are simultaneous superharmonic response, subharmonic response, and combined harmonic response for wind turbine drivetrain, any of which can be combined with any two harmonic responses. By using $\omega_n \approx 2\nu_1 - \nu_2$, and a tuning parameter σ, one has

$$2\nu_1 - \nu_2 = \omega_n + \zeta\sigma \quad (19)$$

The secular term can be removed by setting the coefficient to zero; then the real part and the imaginary part of the derivative for the complex function are opened and set to

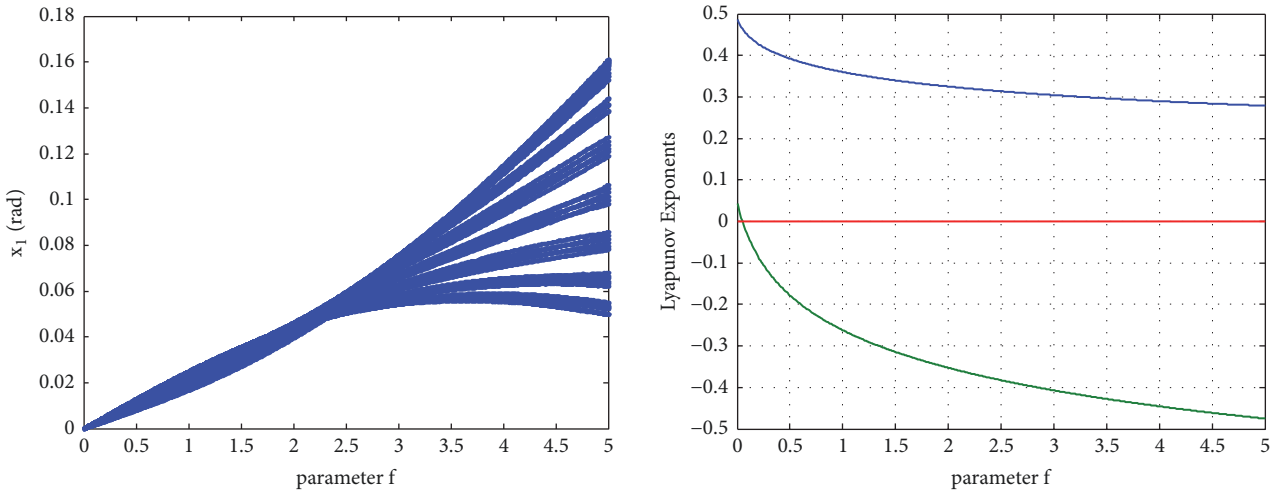

Figure 5: Bifurcation diagram and Lyapunov exponential spectrum.

zero separately; the response amplitude equation is finally expressed as

$$\sigma^2 r^2 + \left[\frac{1}{2}\alpha r - \frac{3}{8}\beta r\left(\omega_n^2 o^2 + 8\Gamma_1^2 + 8\Gamma_2^2\right)\right]^2 = \left(\frac{3}{\omega_n}\beta\Gamma_1\Gamma_2^2\right)^2 \tag{20}$$

where r denote the response amplitude, and $\Gamma_1 = \nu_1\Lambda_1$, $\Gamma_2 = \nu_2\Lambda_2$, $\alpha = a\zeta$, $\beta = b\zeta$.

From (20), it can be concluded that the response amplitude r under the combined harmonic excitation is not only related to the damping coefficient a, b, the amplitude f_i, and the frequency ν_i of the external disturbance excitation, but also related to the tuning parameter σ. so the stability of wind turbine drivetrain is miscellaneous according to various combined excitations.

The Bifurcation diagram and Lyapunov exponent are used to observe the dynamical characteristics of the nonlinear system as the system parameter varies. For a periodic steady state, all Lyapunov exponents of the nonlinear dynamical system are less than zero, whereas at least one more than zero is the signature of a chaotic behavior. Transparently, it is known that, as the amplitude f_i of the external disturbance excitation changes all the time, the running state of the system changes consequentially. As shown in Figure 5, the Bifurcation diagram and Lyapunov exponential spectrum can be described by plotting the maxima of the coordinate φ with parameter f_i varying. Here, $0 < f = f_1 = f_2 < 5, a = -0.15, b = 0.1, k = 1, \nu_1 = 1, \zeta = 0.02, \sigma = 5$, and the initial state are selected as [0.05 0.06].

In accordance with the setting values of the abovementioned system parameters, various numerical computations of the timing diagrams and phase portraits were procured as illustrated in Figure 6, which further validate the occurrence of routes to chaos described in advance. From Figures 5 and 6, the nonlinear dynamical behaviors of the wind turbine drivetrain with combined harmonic excitation are complex, and the system goes through a series of operating states. Although in the sense that chaos is sensitive to initial values and quasirandom and is a transient process in the system, it is still a disadvantage to the stability and security of the whole system. Therefore, in order to assure the system stability, it is very necessary to turn up an approach for controlling the chaotic system to a steady state.

4. Design of Adaptive Fixed-Time Terminal Sliding Mode Controller and Stability Analysis

4.1. Preliminaries. For the global stability analysis, we introduce some necessary lemmas in advance.

Lemma 3 (see [31]). *Assume that there exists a continuous positive definite and radially unbounded function $V(e(t))$ and its right directional derivative satisfies the differential inequality:*

$$\dot{V}(e(t)) + \lambda V^p(e(t)) + \eta V^q(e(t)) \le 0, \quad \forall t \ge t_0,\ e(0) = e_0 \tag{21}$$

where $\lambda, \eta > 0$, $p > 1$, $q < 1$; then the origin of (7) is globally fixed-time stable and the upper bound of settling time $T(e_0)$ can be estimated by

$$\lim_{e_0 \longrightarrow \infty}\left[T(e_0)\right] \le \mathrm{T}_{\max}^1 = \frac{1}{\eta}\left(\frac{\eta}{\lambda}\right)^{(1-q)/(p-q)}\left(\frac{1}{1-q} + \frac{1}{p-1}\right) \tag{22}$$

Lemma 4 (see [19]). *Based on Lemma 3, if $q = 1$, the continuous positive definite and radially unbounded function $V(e(t))$ can be written as follows:*

$$\dot{V}(e(t)) + \lambda V^p(e(t)) + \eta V(e(t)) \le 0, \quad \forall t \ge t_0,\ V(e_0) \ge 0 \tag{23}$$

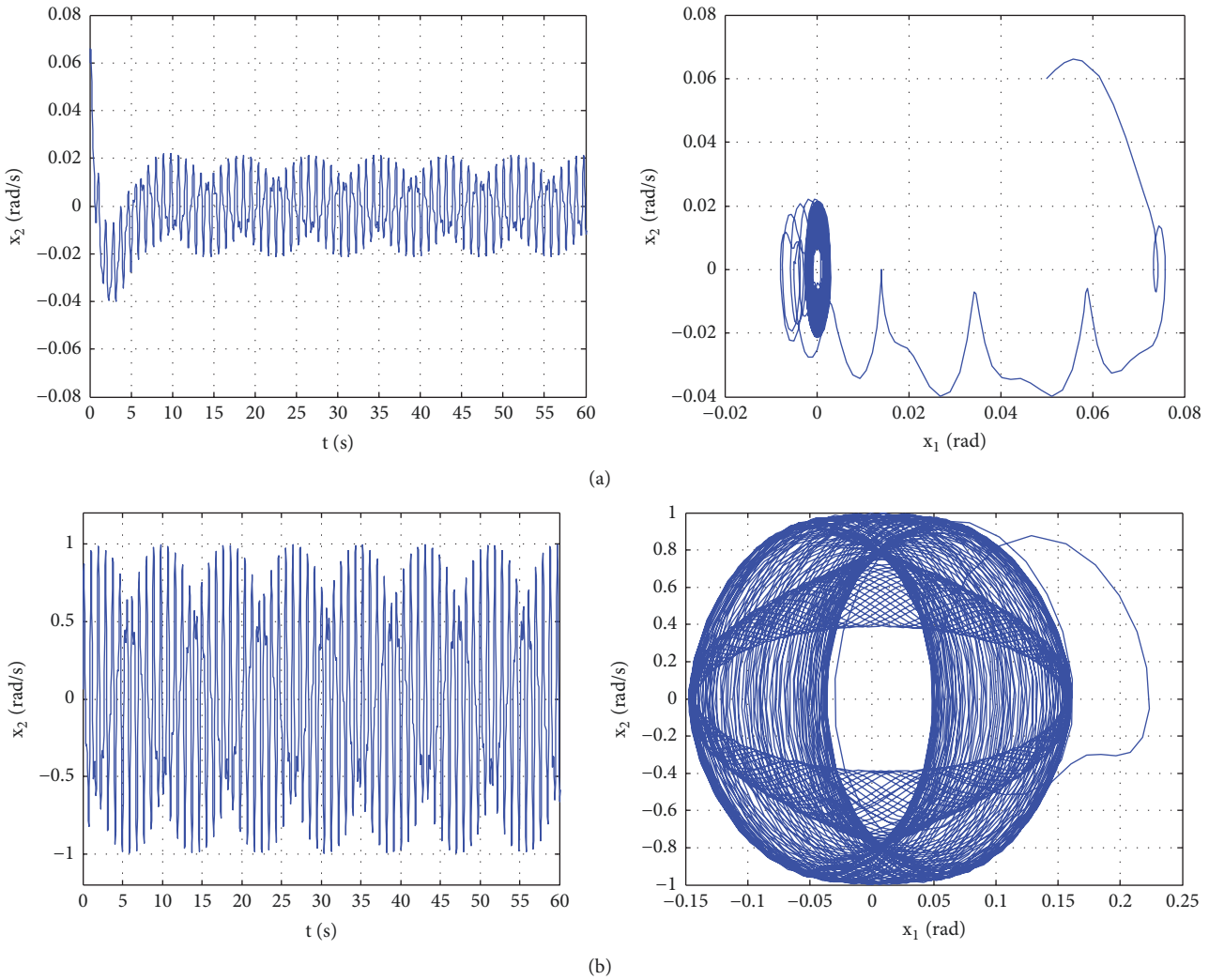

Figure 6: Time domain waveform and phase portrait for different f (a) $f = 0.1$; (b) $f = 5$.

where $\lambda, \eta > 0$, $1 > p > 0$; *it meets* $V(t) \equiv 0$, $\forall t > \mathrm{T}^2_{\max}$. *The convergence time* $\mathrm{T}^2_{\max}$ *is given by* $\mathrm{T}^2_{\max} = t_0 + (1/(1-p)\eta)\mathrm{In}((\lambda + \eta V^{1-p}(e_0))/\lambda)$.

Lemma 5 (see [19]). *From Lemma 4, when* $\eta = 0$, $\forall t \geq t_0$, *the global finite time should be rewritten as* $\mathrm{T}^3_{\max} = t_0 + V^{1-p}(e_0)/(1-p)\lambda$, *and* $T^2_{max} \leq T^3_{max}$ *for* $V(e_0) \geq 0$.

Lemma 6 (see [35]). *If* $\varepsilon_i \in \mathbb{R}, i = 1, 2 \cdots N$ *are arbitrary real numbers, the following inequalities satisfy*

$$\left(\sum_{i=1}^{N} |\varepsilon_i|\right)^{\delta} \leq \sum_{i=1}^{N} |\varepsilon_i|^{\delta}, \quad 0 < \delta \leq 1$$
$$N^{1-\delta}\left(\sum_{i=1}^{N} |\varepsilon_i|\right)^{\delta} \leq \sum_{i=1}^{N} |\varepsilon_i|^{\delta}, \quad 1 < \delta \tag{24}$$

4.2. Design of Adaptive Nonsingular Terminal Sliding Mode Controller. The second-order nonlinear dynamical system is adopted as follows:

$$\begin{aligned} \dot{x}_1 &= x_2 \\ \dot{x}_2 &= f(x,t) + bu(t) + d(t) \\ y &= x_1 \end{aligned} \tag{25}$$

where, according to (6) and (13), $[x_1 \ x_2]^T = [\varphi(t) \ \dot{\varphi}(t)]^T$, $f(x,t) = -ax_2 - bx_2^3 - \omega_n^2 x_1 - kx_1 \cos(\Omega t)$, $d(t) = f_1 \cos(v_1 t) + f_2 \cos(v_2 t)$ denotes the bounded combination harmonic excitation, and $u(t)$ is the control input.

In order to stabilize state variable x_1, let y_d be the desired signal vector. The control error and its derivatives are written as $e_1 = y - y_d$ and $e_2 = \dot{y} - \dot{y}_d$. From (25), one has

$$\begin{aligned} \dot{e}_1 &= e_2 \\ \dot{e}_2 &= F(x) + Bu(t) + D(t) \end{aligned} \tag{26}$$

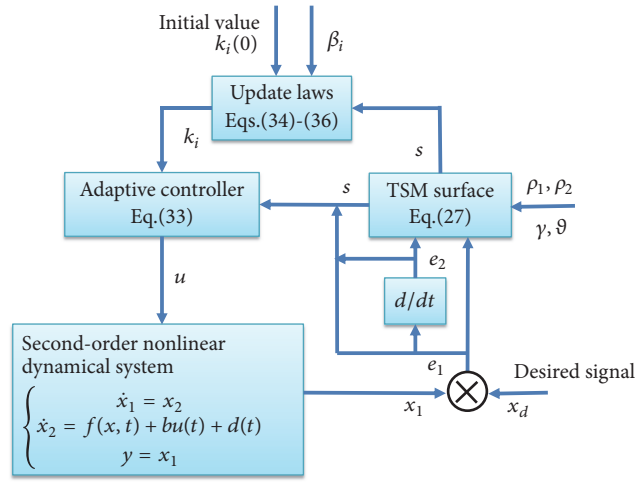

FIGURE 7: Control flowchart diagram of closed loop system.

where $F(x) = f(x,t) - \ddot{y}_d$, $B = b$, $D(t) = d(t)$, and there is the bounded condition $|D(t)| \le \beta_0, \beta_0$ is the given constant.

Then the proposed nonsingular terminal sliding mode manifold can be described as

$$s(t) = e_2 + \left(\gamma |e_1|^{\rho_1} + \vartheta |e_1|^{\rho_2}\right) \operatorname{sign}(e_1) \tag{27}$$

where $\gamma, \vartheta > 0$ and $0 \le \rho_2 < 1, \rho_1 > 1$; by using $(d/dt)(|e_1|^{\chi} \operatorname{sign}(e_1)) = \chi |e_1|^{\chi-1} \dot{e}_1$, the time derivative of (27) can be derived as

$$\dot{s}(t) = \dot{e}_2 + \left(\gamma\rho_1 |e_1|^{\rho_1-1} + \vartheta\rho_2 |e_1|^{\rho_2-1}\right) \dot{e}_1 \tag{28}$$

According to the sliding mode control theory, the sliding mode manifold and its derivative must satisfy

$$\begin{aligned} s(t) &= 0 \\ \text{and } \dot{s}(t) &= 0 \end{aligned} \tag{29}$$

By substituting (26) without combination harmonic excitation into (28), one can have

$$\begin{aligned} \dot{s}(t) &= F(x) + Bu_{eq}(t) \\ &\quad + \left(\gamma\rho_1 |e_1|^{\rho_1-1} + \vartheta\rho_2 |e_1|^{\rho_2-1}\right) e_2 \end{aligned} \tag{30}$$

From (29), the equivalent control law u_{eq} can be obtained as

$$u_{eq} = B^{-1}\left[-F(x) - \left(\gamma\rho_1 |e_1|^{\rho_1-1} + \vartheta\rho_2 |e_1|^{\rho_2-1}\right) e_2\right] \tag{31}$$

In order to satisfy the sliding condition in the presence of combination harmonic excitation, a switching adaptive law u_{sw} is designed as

$$u_{sw} = -B^{-1}\left[\left(k_1 |s|^{\rho_3} + k_2 |s|^{\rho_4}\right) + k_0\right] \operatorname{sign}(s) \tag{32}$$

where $0 \le \rho_4 < 1$, $\rho_3 > 1$, and k_i, $i = 0, 1, 2$, are the estimations of the tuning parameters. Then, the overall sliding mode control law can be given below

$$\begin{aligned} u &= u_{eq} + u_{sw} \\ &= B^{-1}\left\{\begin{array}{c}\left[-F(x) - \left(\gamma\rho_1 |e_1|^{\rho_1-1} + \vartheta\rho_2 |e_1|^{\rho_2-1}\right) e_2\right] \\ -\left[\left(k_1 |s|^{\rho_3} + k_2 |s|^{\rho_4}\right) + k_0\right] \operatorname{sign}(s)\end{array}\right\} \end{aligned} \tag{33}$$

The estimations of the parameters k_0, k_1, and k_2 are updated by the following adaptive laws:

$$\begin{aligned} \dot{k}_0 &= \left[|s| \right. \\ &\quad \left. - \left(\beta_1 |k_0 - \beta_0|^{\rho_3} + \beta_2 |k_0 - \beta_0|^{\rho_4}\right) \operatorname{sign}(k_0 - \beta_0)\right] \end{aligned} \tag{34}$$

$$\begin{aligned} \dot{k}_1 &= \left[|s|^{\rho_3+1} \right. \\ &\quad \left. - \left(\beta_1 |k_1 - \beta_1|^{\rho_3} + \beta_2 |k_1 - \beta_1|^{\rho_4}\right) \operatorname{sign}(k_1 - \beta_1)\right] \end{aligned} \tag{35}$$

$$\begin{aligned} \dot{k}_2 &= \left[|s|^{\rho_4+1} \right. \\ &\quad \left. - \left(\beta_1 |k_2 - \beta_2|^{\rho_3} + \beta_2 |k_2 - \beta_2|^{\rho_4}\right) \operatorname{sign}(k_2 - \beta_2)\right] \end{aligned} \tag{36}$$

where β_0, β_1, and β_2 are the arbitrary constants. The control flowchart diagram of closed loop system is illustrated in Figure 7.

4.3. Fixed-Time Stability Analysis. In this section, some main results of the proposed adaptive fixed-time terminal sliding mode control are analytically proved in the following theorem.

Theorem 7. *The adaptive controller of system (25) is designed as (33) and the corresponding updated laws are chosen as (34)-(36). If the sliding mode manifold is expressed as (27), then the*

system state trajectories converge to the sliding surface within a finite time bounded by

$$t_r \le \frac{2^{(1-\rho_4)/2}}{\beta_2}\left(\frac{2^{(\rho_4-\rho_3)/2}\beta_2}{2\beta_1}\right)^{(1-\rho_4)/(\rho_3-\rho_4)} \cdot\left(\frac{1}{1-\rho_4}+\frac{1}{\rho_3-1}\right) \tag{37}$$

Proof. The Lyapunov function candidate is constructed as follows:

$$V_1 = \frac{1}{2}s(t)^T s(t) + \frac{1}{2}\sum_{i=0}^{2}(k_i-\beta_i)^2 \tag{38}$$

Then the time derivative of V_1 can be written as

$$\dot{V}_1 = s(t)\begin{pmatrix} F(x)+Bu(t)+D(t) \\ +\left(\gamma\rho_1|e_1|^{\rho_1-1}+\vartheta\rho_2|e_1|^{\rho_2-1}\right)e_2\end{pmatrix} + \sum_{i=0}^{2}(k_i-\beta_i)\dot{k}_i \tag{39}$$

Substituting the designed control law u (33) into (39), one gets

$$\dot{V}_1 = s(t)\left[D(t)-\left(\left(k_1|s|^{\rho_3}+k_2|s|^{\rho_4}\right)+k_0\right)\operatorname{sign}(s)\right] + \sum_{i=0}^{2}(k_i-\beta_i)\dot{k}_i \tag{40}$$

Combining the adaptive updating laws (34)-(36), one has

$$\begin{aligned}\dot{V}_1 &= D(t)s - k_1|s|^{\rho_3+1} - k_2|s|^{\rho_4+1} - k_0|s| \\ &\quad + (k_0-\beta_0)\cdot\left[|s| - \begin{pmatrix}\beta_1|k_0-\beta_0|^{\rho_3} \\ +\beta_2|k_0-\beta_0|^{\rho_4}\end{pmatrix}\operatorname{sign}(k_0-\beta_0)\right] \\ &\quad + (k_1-\beta_1)\cdot\left[|s|^{\rho_3+1} - \begin{pmatrix}\beta_1|k_1-\beta_1|^{\rho_3} \\ +\beta_2|k_1-\beta_1|^{\rho_4}\end{pmatrix}\operatorname{sign}(k_1-\beta_1)\right] \\ &\quad + (k_2-\beta_2)\cdot\left[|s|^{\rho_4+1} - \begin{pmatrix}\beta_1|k_2-\beta_2|^{\rho_3} \\ +\beta_2|k_2-\beta_2|^{\rho_4}\end{pmatrix}\operatorname{sign}(k_2-\beta_2)\right]\end{aligned} \tag{41}$$

To simplify the calculation, the above equation is modified as

$$\begin{aligned}\dot{V}_1 &= D(t)s - \beta_0|s| - \begin{pmatrix}\beta_1|k_0-\beta_0|^{\rho_3+1} \\ +\beta_2|k_0-\beta_0|^{\rho_4+1}\end{pmatrix} \\ &\quad - \beta_1|s|^{\rho_3+1} - \begin{pmatrix}\beta_1|k_1-\beta_1|^{\rho_3+1} \\ +\beta_2|k_1-\beta_1|^{\rho_4+1}\end{pmatrix} - \beta_2|s|^{\rho_4+1} \\ &\quad - \begin{pmatrix}\beta_1|k_2-\beta_2|^{\rho_3+1} \\ +\beta_2|k_2-\beta_2|^{\rho_4+1}\end{pmatrix} \le (|D(t)|-\beta_0)|s| \\ &\quad - \beta_1\left(|s|^{\rho_3+1}+|k_0-\beta_0|^{\rho_3+1}+|k_1-\beta_1|^{\rho_3+1}\right. \\ &\quad \left.+|k_2-\beta_2|^{\rho_3+1}\right) - \beta_2\left(|s|^{\rho_4+1}+|k_0-\beta_0|^{\rho_4+1}\right. \\ &\quad \left.+|k_1-\beta_1|^{\rho_4+1}+|k_2-\beta_2|^{\rho_4+1}\right)\end{aligned} \tag{42}$$

According to Lemma 6, it is easy to obtain that

$$\begin{aligned}\dot{V}_1 &\le -2^{(\rho_3+1)/2}\beta_1\left(\left(\frac{1}{2}s^2\right)^{(\rho_3+1)/2}\right. \\ &\quad \left.+\left(\frac{1}{2}(k_0-\beta_0)^2\right)^{(\rho_3+1)/2}+\left(\frac{1}{2}(k_1-\beta_1)^2\right)^{(\rho_3+1)/2}\right. \\ &\quad \left.+\left(\frac{1}{2}(k_2-\beta_2)^2\right)^{(\rho_3+1)/2}\right) \\ &\quad - 2^{(\rho_4+1)/2}\beta_2\left(\left(\frac{1}{2}s^2\right)^{(\rho_4+1)/2}\right. \\ &\quad \left.+\left(\frac{1}{2}(k_0-\beta_0)^2\right)^{(\rho_4+1)/2}+\left(\frac{1}{2}(k_1-\beta_1)^2\right)^{(\rho_4+1)/2}\right. \\ &\quad \left.+\left(\frac{1}{2}(k_2-\beta_2)^2\right)^{(\rho_4+1)/2}\right) \\ &\le -4^{1-(\rho_3+1)/2}2^{(\rho_3+1)/2}\beta_1\left(\frac{1}{2}s(t)^T s(t)\right. \\ &\quad \left.+\frac{1}{2}\sum_{i=0}^{2}(k_i-\beta_i)^2\right)^{(\rho_3+1)/2} \\ &\quad - 2^{(\rho_4+1)/2}\beta_2\left(\frac{1}{2}s(t)^T s(t)\right. \\ &\quad \left.+\frac{1}{2}\sum_{i=0}^{2}(k_i-\beta_i)^2\right)^{(\rho_4+1)/2} = -2^{(3-\rho_3)/2}\beta_1 V_1^{(\rho_3+1)/2} \\ &\quad - 2^{(\rho_4+1)/2}\beta_2 V_1^{(\rho_4+1)/2}\end{aligned} \tag{43}$$

It follows from Lemma 3 that system (25) can be globally fixed time stable and the settling time is upper bounded by (37).The proof is completed. □

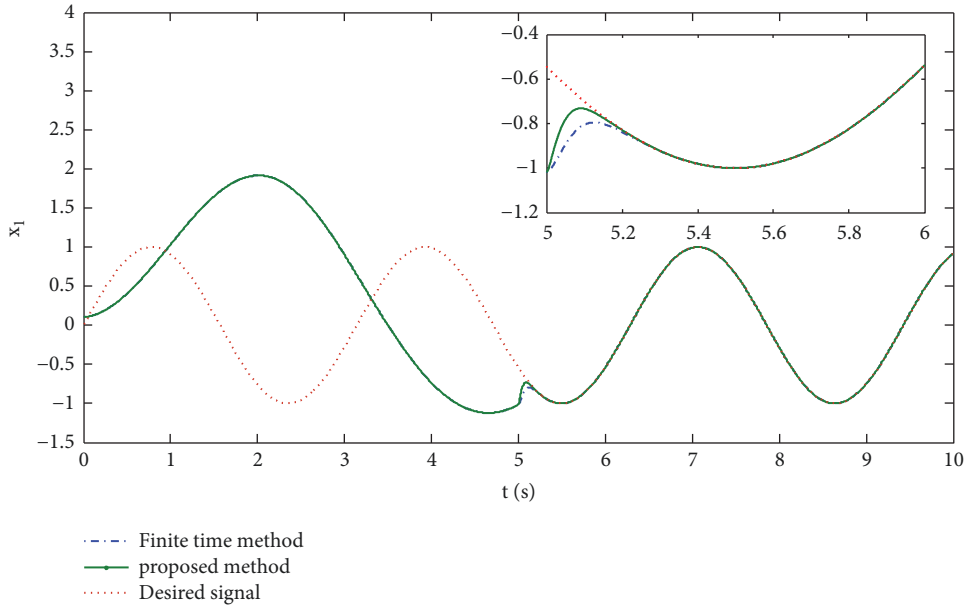

Figure 8: Time response of tracking x_1.

When the error variables are on the sliding manifold, their dynamics will meet ($s(t) = 0$)

$$e_2 = -\left(\gamma |e_1|^{\rho_1} + \vartheta |e_1|^{\rho_2}\right) \operatorname{sign}(e_1) \tag{44}$$

Theorem 8. *The sliding mode dynamics (44) of the error system (26) is finite time stable and its state trajectories globally converge to the origin with the settling time upper bounded by*

$$t_s \le \frac{2^{(1-\rho_2)/2}}{\vartheta}\left(\frac{2^{(\rho_2-\rho_1)/2}\vartheta}{\gamma}\right)^{(1-\rho_2)/(\rho_1-\rho_2)} \cdot \left(\frac{1}{1-\rho_2} + \frac{1}{\rho_1 - 1}\right) \tag{45}$$

Proof. The Lyapunov candidate function is selected in the following form:

$$V_2(t) = \frac{1}{2}e_1^2(t) \tag{46}$$

From (44), one can get

$$\begin{aligned} \dot{V}_2(t) &= e_1\dot{e}_1 \\ &= -e_1\left(\gamma |e_1|^{\rho_1} + \vartheta |e_1|^{\rho_2}\right) \operatorname{sign}(e_1) - \gamma |e_1|^{\rho_1+1} \\ &\quad - \vartheta |e_1|^{\rho_2+1} \\ &= -2^{(\rho_1+1)/2}\gamma V_2^{(\rho_1+1)/2} - 2^{(\rho_2+1)/2}\vartheta V_2^{(\rho_2+1)/2} \end{aligned} \tag{47}$$

In the light of Lemma 3, the upper bound of convergence time can be estimated by (45). The proof is completed. □

5. Simulation Results

In this section, numerical simulation results are used to validate the effectiveness and the superiority of the proposed control algorithm for the system (25). The system parameters are selected as $0 < f = f_1 = f_2 < 5, a = -0.15, b = 0.1, k = 1$, $\nu_1 = 1$; the controller parameters are chosen as $\gamma = \vartheta = 10$, $\rho_1 = 1.5$, $\rho_2 = 0.5$, $k_0(0) = k_1(0) = k_2(0) = 3$, $\beta_0 = 2.5$, $\beta_1 = 10$, $\beta_2 = 8$, $\rho_3 = 1.8$, $\rho_4 = 0.5$. Based on Lemma 3, by calculation from (37) and (45), the estimation upper bound of convergence time can be obtained by $T_{max}^1 < t_r + t_s = 0.2856 + 0.4 = 0.6856s$.

In numerical simulation, to highlight the superiorities of the proposed scheme in further depth, two cases of the reference signal are implemented in keeping the rest of conditions unchanged.

Case 1. The reference signal is chosen as $x_d(t) = \sin(2t)$.

Case 2. The reference signal is set as $x_d(t) = \sin(\pi t)$.

The initial conditions of the state variable are set as $[x_1(0), x_2(0)] = [0.1\ 0.12]$. According to Lemma 4, the tuning parameters of the finite-time method are designed as $\lambda = 8$, $\eta = 10$, $p = 0.5$. After calculation, one can get $T_{max}^2 \le 0.9206$. The controller is activated at $t = 5s$. As shown in Figures 8 and 9, the response curves of state variables with Case 1 accurately track the reference signal. By comparing the proposed scheme, one can see that the convergence time is shorter than the finite-time method and the chattering phenomenon is well suppressed. As illustrated in Figure 10, the estimated values of tuning parameters k_0, k_1, and k_2 will fast converge to β_0, β_1, β_2, respectively.

In order to exhibit the merits of the proposed fixed-time method, the control effect is independent of the initial

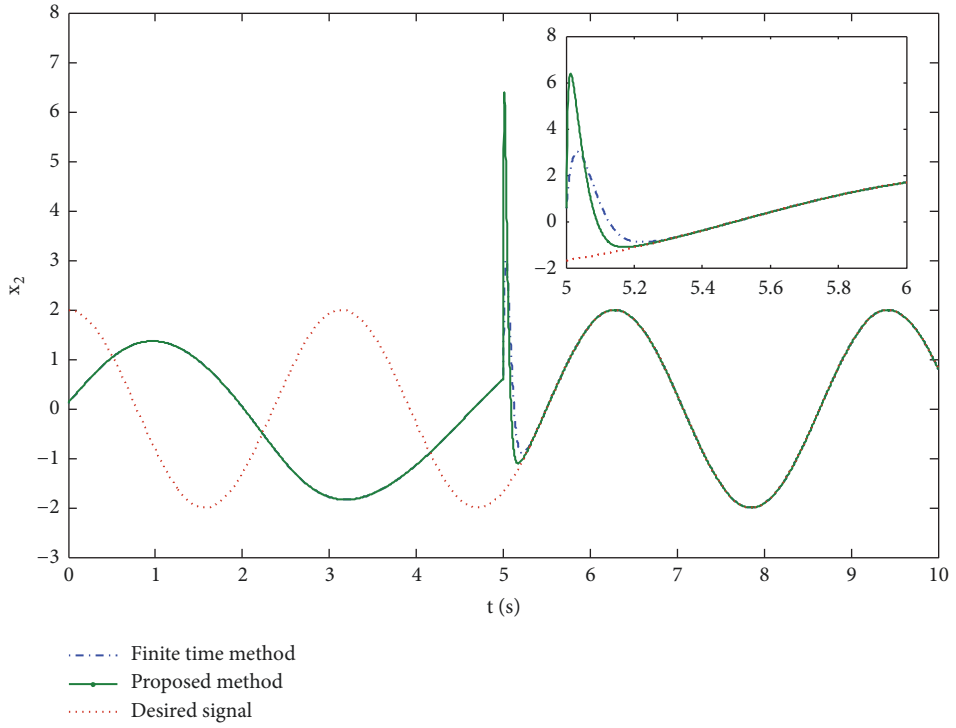

Figure 9: The curve of tracking x_2.

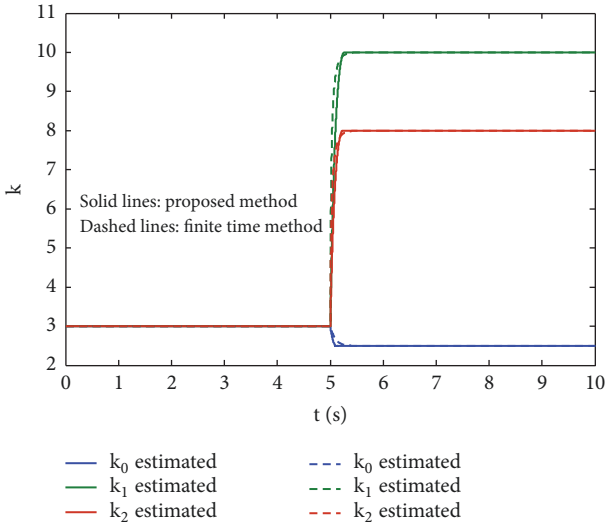

Figure 10: The tuning parameter estimations.

conditions. Therefore, in case 2, the initial conditions of the state variable are set as $[x_1(0), x_2(0)] = [0.15\ 0.22]$. According to Lemma 4, the tuning parameters of the finite-time method are designed as $\lambda = 5$, $\eta = 8$, $p = 0.5$. After calculation, one can get $T^2_{max} \leq 1.140s$. As illustrated in Figures 11 and 12, adding proposed controller at $t = 8s$, the state variables rapidly stabilize to the certain value. Meanwhile, the comparative results explore the shorter stabilization time and the free chattering phenomenon in simulation. When $k_0(0) = k_1(0) = k_2(0) = 5$, the estimated values of tuning parameters k_0, k_1, and k_2 are demonstrated in Figure 13.

6. Conclusions

In this study, the stability analysis of a complex nonlinear drivetrain with combined harmonic excitation can be addressed by relying on nonlinear dynamics theory. First, we rebuilt the mathematical model of the wind turbine drivetrain considering the nonlinear time-varying stiffness and the

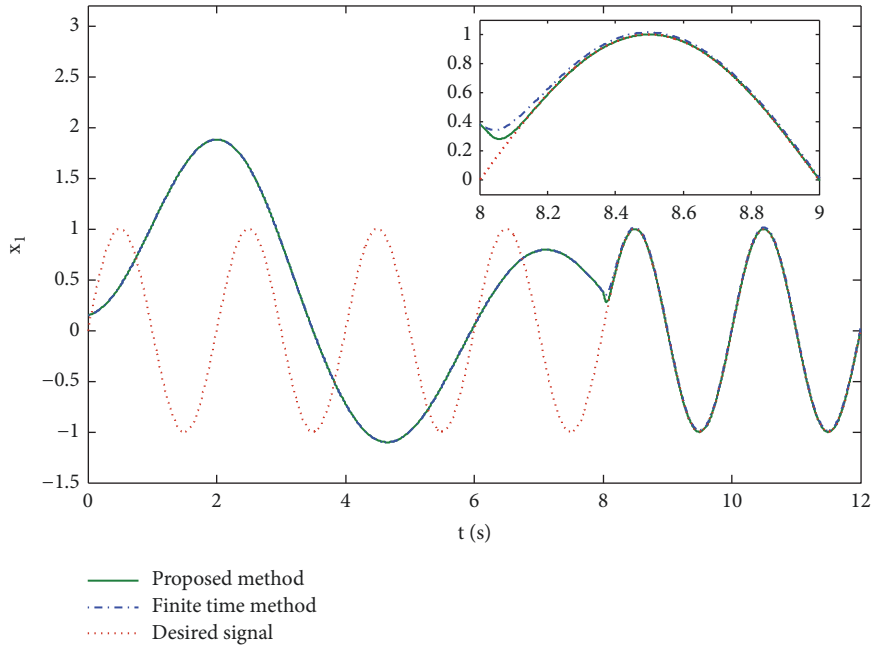

Figure 11: Time response of tracking x_1.

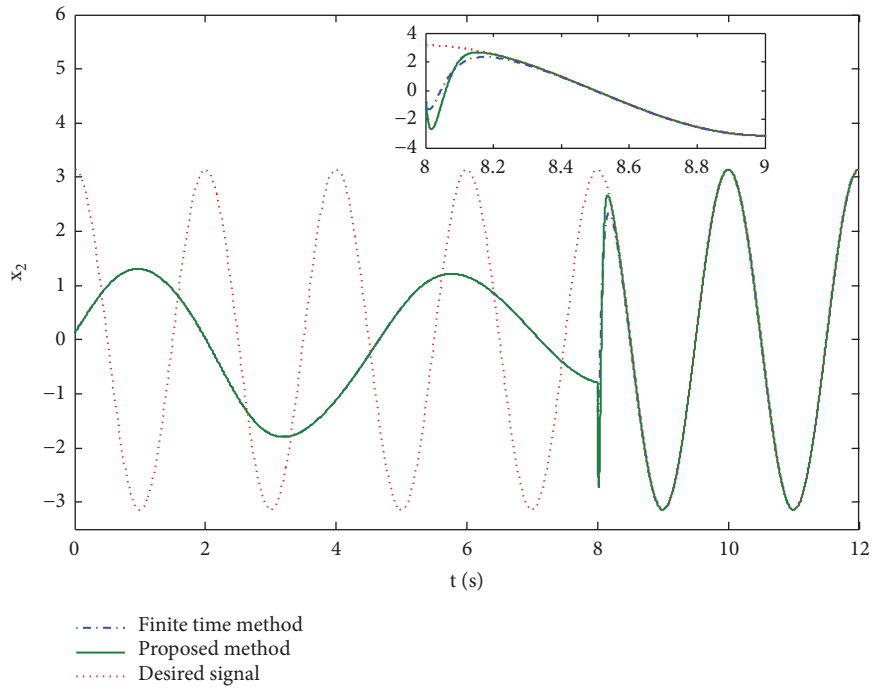

Figure 12: The curve of tracking x_2.

nonlinear damping force. Second, the nonlinear dynamics theory is introduced to analyze the stability of the wind turbine drivetrain including bifurcation map, phase diagrams, and Lyapunov exponential spectrum under combined harmonic excitation. Then, numerical results clearly show that the greater the amplitude of the external disturbance excitation, the smaller the damping, and the larger the value of the nonlinear negative stiffness, the more unstable the wind turbine drivetrain. In order to guarantee the stability and normal functioning of the whole system, an adaptive fixed-time terminal sliding mode control approach can be implemented. Finally, in comparison with finite-time method, the applicability and superiority of the proposed scheme can be exhibited by numerical simulations, which are in good agreement with the theoretical analysis for the vibration phenomena of the wind turbine drivetrain. Meanwhile, it is

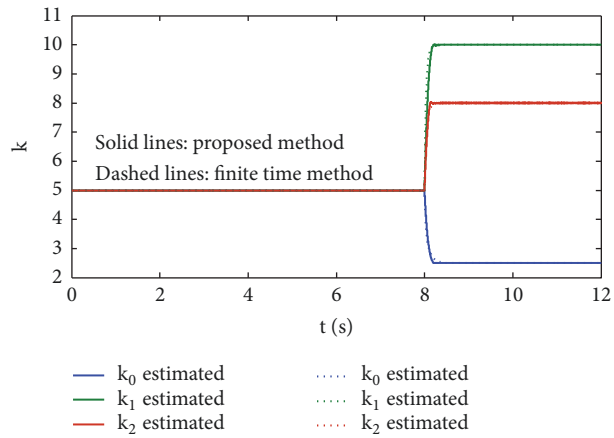

FIGURE 13: The estimations of tuning parameter k_i $(i = 0, 1, 2)$.

noteworthy that the proposed method here can be further extended to the steady operation and design of the dual-motor driving electromechanical system. The fixed-time sliding mode control with an adaptive disturbance observer for the high-order or fractional-order dynamic system can be considered to estimate the model uncertainty directly in the future work.

Data Availability

The data used to support the findings of this study are included within the article.

Conflicts of Interest

The authors declare that there are no conflicts of interest regarding the publication of this paper.

Acknowledgments

This wok was supported by the National Natural Science Foundation of People's Republic of China (Grant no. 51075326) and the Basic Ability Enhancement Project of Young Teachers in Guangxi Provincial Department of Education (Grant no. KY2015YB305).

References

[1] S. Ganjefar and A. A. Ghasemi, "A novel-strategy controller design for maximum power extraction in stand-alone windmill systems," *Energy*, vol. 76, pp. 326–335, 2014.

[2] D. Song, J. Yang, M. Su, A. Liu, Y. Liu, and Y. H. Joo, "A comparison study between two MPPT control methods for a large variable-speed wind turbine under different wind speed characteristics," *Energies*, vol. 10, no. 5, p. 613, 2017.

[3] C. Huang, F. Li, and Z. Jin, "Maximum power point tracking strategy for large-scale wind generation systems considering wind turbine dynamics," *IEEE Transactions on Industrial Electronics*, vol. 62, no. 4, pp. 2530–2539, 2015.

[4] B. Boukhezzar and H. Siguerdidjane, "Nonlinear control of a variable-speed wind turbine using a two-mass model," *IEEE Transactions on Energy Conversion*, vol. 26, no. 1, pp. 149–162, 2011.

[5] J. Chen and Y. Song, "Dynamic loads of variable-speed wind energy conversion system," *IEEE Transactions on Industrial Electronics*, vol. 63, no. 1, pp. 178–188, 2016.

[6] I. P. Girsang, J. S. Dhupia, E. Muljadi, M. Singh, and J. Jonkman, "Modeling and control to mitigate resonant load in variable-speed wind turbine drivetrain," *IEEE Journal of Emerging and Selected Topics in Power Electronics*, vol. 1, no. 4, pp. 277–286, 2013.

[7] H. Geng and D. Xu, "Stability analysis and improvements for variable-speed multipole permanent magnet synchronous generator-based wind energy conversion system," *IEEE Transactions on Sustainable Energy*, vol. 2, no. 4, pp. 459–467, 2011.

[8] J. Chen, J. Chen, and C. Gong, "On optimizing the aerodynamic load acting on the turbine shaft of pmsg-based direct-drive wind energy conversion system," *IEEE Transactions on Industrial Electronics*, vol. 61, no. 8, pp. 4022–4031, 2014.

[9] M. Rahimi, "Modeling, control and stability analysis of grid connected PMSG based wind turbine assisted with diode rectifier and boost converter," *International Journal of Electrical Power & Energy Systems*, vol. 93, pp. 84–96, 2017.

[10] D. Xie, Y. Lu, J. Sun, and C. Gu, "Small signal stability analysis for different types of PMSGs connected to the grid," *Journal of Renewable Energy*, vol. 106, Supplement C, pp. 149–164, 2017.

[11] M. Rahimi, "Improvement of energy conversion efficiency and damping of wind turbine response in grid connected DFIG based wind turbines," *International Journal of Electrical Power & Energy Systems*, vol. 95, pp. 11–25, 2018.

[12] P. Srikanth and A. Sekhar, "Wind turbine drive train dynamic characterization using vibration and torque signals," *Mechanism and Machine Theory*, vol. 98, pp. 2–20, 2016.

[13] M. Rahimi, "Drive train dynamics assessment and speed controller design in variable speed wind turbines," *Journal of Renewable Energy*, vol. 89, pp. 716–729, 2016.

[14] S. M. Muyeen, M. H. Ali, R. Takahashi et al., "Comparative study on transient stability analysis of wind turbine generator system using different drive train models," *IET Renewable Power Generation*, vol. 1, no. 2, pp. 131–141, 2007.

[15] C. Pradhan, C. N. Bhende, and A. K. Samanta, "Adaptive virtual inertia-based frequency regulation in wind power systems," *Journal of Renewable Energy*, vol. 115, Supplement C, pp. 558–574, 2018.

[16] Z. Meng, L.-Y. Fu, and M.-H. Song, "Bifurcation of a kind of nonlinear-relative rotational system with combined harmonic excitation," *Acta Physica Sinica*, vol. 62, no. 5, 2013.

[17] Y. Liu, L. Sun, J. Lu, and J. Liang, "Feedback controller design for the synchronization of Boolean control networks," *IEEE Transactions on Neural Networks and Learning Systems*, vol. 27, no. 9, pp. 1991–1996, 2016.

[18] D. Chen, S. Liu, and X. Ma, "Modeling, nonlinear dynamical analysis of a novel power system with random wind power and it's control," *Energy*, vol. 53, pp. 139–146, 2013.

[19] D. Zhang, J. Mei, and P. Miao, "Global finite-time synchronization of different dimensional chaotic systems," *Applied Mathematical Modelling: Simulation and Computation for Engineering and Environmental Systems*, vol. 48, pp. 303–315, 2017.

[20] B. Torchani, A. Sellami, and G. Garcia, "Variable speed wind turbine control by discrete-time sliding mode approach," *ISA Transactions®*, vol. 62, pp. 81–86, 2016.

[21] J. Sun, Y. Wang, Y. Wang, and Y. Shen, "Finite-time synchronization between two complex-variable chaotic systems with unknown parameters via nonsingular terminal sliding mode control," *Nonlinear Dynamics*, vol. 85, no. 2, pp. 1105–1117, 2016.

[22] J. Sun, Y. Wu, G. Cui, and Y. Wang, "Finite-time real combination synchronization of three complex-variable chaotic systems with unknown parameters via sliding mode control," *Nonlinear Dynamics*, vol. 88, no. 3, pp. 1677–1690, 2017.

[23] F. Yang, J. Mei, and Z. Wu, "Finite-time synchronisation of neural networks with discrete and distributed delays via periodically intermittent memory feedback control," *IET Control Theory & Applications*, vol. 10, no. 14, pp. 1630–1640, 2016.

[24] A. Polyakov, "Nonlinear feedback design for fixed-time stabilization of linear control systems," *IEEE Transactions on Automatic Control*, vol. 57, no. 8, pp. 2106–2110, 2012.

[25] Z. Zuo, "Nonsingular fixed-time consensus tracking for second-order multi-agent networks," *Automatica*, vol. 54, pp. 305–309, 2015.

[26] J. Ni, L. Liu, C. Liu, X. Hu, and S. Li, "Fast fixed-time nonsingular terminal sliding mode control and its application to chaos suppression in power system," *IEEE Transactions on Circuits and Systems II: Express Briefs*, vol. 64, no. 2, pp. 151–155, 2017.

[27] J. Wang, C. Liu, Y. Wang, and G. Zheng, "Fixed time integral sliding mode controller and its application to the suppression of chaotic oscillation in power system," *Chinese Physics B*, vol. 27, no. 7, p. 070503, 2018.

[28] M. Liu, J. Wu, and Y.-Z. Sun, "Fixed-time stability analysis of permanent magnet synchronous motors with novel adaptive control," *Mathematical Problems in Engineering*, vol. 2017, Article ID 4903963, 11 pages, 2017.

[29] C. Ma, F. Wang, Z. Li et al., "Adaptive fixed-time fast terminal sliding mode control for chaotic oscillation in power system," *Mathematical Problems in Engineering*, vol. 2018, Article ID 5819428, 10 pages, 2018.

[30] M. Boukattaya, N. Mezghani, and T. Damak, "Adaptive nonsingular fast terminal sliding-mode control for the tracking problem of uncertain dynamical systems," *ISA Transactions®*, vol. 77, pp. 1–19, 2018.

[31] C. Hu, J. Yu, Z. Chen, H. Jiang, and T. Huang, "Fixed-time stability of dynamical systems and fixed-time synchronization of coupled discontinuous neural networks," *Neural Networks*, vol. 89, pp. 74–83, 2017.

[32] H. Geng, D. Xu, B. Wu, and G. Yang, "Active damping for PMSG-based WECS with DC-link current estimation," *IEEE Transactions on Industrial Electronics*, vol. 58, no. 4, pp. 1110–1119, 2011.

[33] J. Sun, X. Zhao, J. Fang, and Y. Wang, "Autonomous memristor chaotic systems of infinite chaotic attractors and circuitry realization," *Nonlinear Dynamics*, vol. 94, no. 4, pp. 2879–2887, 2018.

[34] P. Shi, J. Li, J. Jiang, B. Liu, and D. Han, "Nonlinear dynamics of torsional vibration for rolling Mill's main drive system under parametric excitation," *Journal of Iron and Steel Research, International*, vol. 20, no. 1, pp. 7–12, 2013.

[35] J. Ni, L. Liu, C. Liu, and X. Hu, "Fractional order fixed-time nonsingular terminal sliding mode synchronization and control of fractional order chaotic systems," *Nonlinear Dynamics*, vol. 89, no. 3, pp. 2065–2083, 2017.